Time-Resolved Fluorescence Study of the Single Tryptophans of Engineered Skeletal Muscle Troponin C

Mingda She,* Wen-Ji Dong,# Patrick K. Umeda,§ and Herbert C. Cheung*#
Departments of *Physics, #Biochemistry and Molecular Genetics, and §Medicine, University of Alabama at Birmingham, Birmingham, Alabama 35294 USA

ABSTRACT The regulatory domain of troponin C (TnC) from chicken skeletal muscle was studied using genetically generated mutants which contained a single tryptophan at positions 22, 52, and 90. The quantum yields of Trp-22 are 0.33 and 0.25 in the presence of Mg^{2+} (2-Mg state) and Ca^{2+} (4-Ca state), respectively. The large quantum yield of the 2-Mg state is due to a relatively small nonradiative decay rate and consistent with the emission peak at 331 nm. The intensity decay of this state is monoexponential with a single lifetime of 5.65 ns, independent of wavelength. In the 4-Ca state, the decay is biexponential with the mean of the two lifetimes increasing from 4.54 to 4.92 ns across the emission band. The decay-associated spectrum of the short lifetime is red-shifted by 19 nm relative to the steady-state spectrum. The decay of Trp-52 is biexponential in the 2-Mg state and triexponential in the 4-Ca state. The decay of Trp-90 requires three exponential terms for a satisfactory fit, but can be fitted with two exponential terms in the 4-Ca state. The lower quantum yields (<0.15) of these two tryptophans are due to a combination of smaller radiative and larger nonradiative decay rates. The results from Trp-22 suggest a homogeneous ground-state indole ring in the absence of bound Ca^{2+} at the regulatory sites and a ground-state heterogeneity induced by activator Ca^{2+}. The Ca^{2+}-induced environmental changes of Trp-52 and Trp-90 deviate from those predicted by a modeled structure of the 4-Ca state. The anisotropy decays of all three tryptophans show two rotational correlation times. The long correlation times (ϕ_1 = 8.1–8.3 ns) derived from Trp-22 and Trp-90 suggest an asymmetric hydrodynamic shape. TnC becomes more asymmetric upon binding activator Ca^{2+} (ϕ_1 = 10.1–11.6 ns). The values of ϕ_1 obtained from Trp-52 are 3–4 ns shorter than those from Trp-22 and Trp-90, and these reduced correlation times may be related to the mobility of the residue and/or local segmental flexibility.

INTRODUCTION

In striated muscle, the thin filament consists of polymerized actin, which is decorated with the regulatory proteins troponin and tropomyosin. Cyclic interactions between the thin filament and the myosin cross-bridges of the thick filament lead to cycles of contraction and relaxation. The initial molecular event leading to regulation of actomyosin ATPase and force generation involves reversible binding of Ca^{2+} to troponin C (TnC), one of the three subunits of troponin. The Ca^{2+} signal is then transmitted to the other two subunits, troponin I (TnI) and troponin T, via a series of conformational changes initially induced in TnC. The interaction between TnC and TnI from vertebrate skeletal muscle has a moderate affinity in the absence of Ca^{2+} bound to TnC and becomes enhanced by several orders of magnitude if TnC is already fully saturated with Ca^{2+}. This Ca^{2+}-induced enhanced affinity is generally believed to be the thermodynamic basis of a Ca^{2+} switch that triggers contraction (Cheung et al., 1987; Tao et al., 1990). The structural basis of this switch is not well understood.

TnC is a single-polypeptide protein with a molecular weight of ~18,000. The isoform from vertebrate skeletal muscle has four active sites for Ca^{2+}. Sites 1 and 2, located on the N-terminal segment of the polypeptide, bind Ca^{2+} specifically with a low affinity ($\sim 5 \times 10^5\ M^{-1}$) (Potter and Gergely, 1975); sites 3 and 4, located on the C-terminal segment, bind Ca^{2+} with a high affinity ($\sim 2 \times 10^7\ M^{-1}$) and also bind Mg^{2+} ($\sim 5 \times 10^3\ M^{-1}$) competitively (Leavis et al., 1978). In relaxed muscle, the two Ca/Mg sites are likely saturated with Mg^{2+} because of the high intracellular Mg^{2+} concentration, but the two Ca^{2+}-specific sites are unoccupied. It is the binding of Ca^{2+} to the two low-affinity sites that is involved in Ca^{2+} regulation. The x-ray structure of TnC from skeletal muscle shows the protein to have an elongated dumbbell shape in which the N-terminal and C-terminal segments are each folded into a globular domain (Herzberg and James, 1985; Sundaralingam et al., 1985). The two domains are connected by an α-helix exposed to solvent. This structure contains two bound Ca^{2+} at the Ca/Mg sites in the C-domain (2-Ca structure), but is devoid of bound Ca^{2+} at the two regulatory sites. The Ca^{2+}-saturated C-domain has two typical EF-hand motifs (Kretsinger and Nockolds, 1973) in which a Ca^{2+} is coordinated to a 12-residue loop flanked by two helices that are oriented relative to each other at an angle of ~90°. Because of the absence of bound cation in the N-domain, the orientations of the two sets of helix-loop-helix deviate from the typical EF-hand motif. It has been proposed that the two regulatory sites will adopt typical EF-hand conformations upon satu-

Received for publication 18 February 1997 and in final form 11 May 1997.

Address reprint requests to H. C. Cheung, Department of Biochemistry and Molecular Genetics, Room 520, CHSB-19, University of Alabama at Birmingham, Birmingham, AL 35294-2041. Tel.: 205-934-2485; Fax: 205-975-4621; E-mail: hccheung@bmg.bhs.uab.edu.

Materials presented in this publication are part of the Ph.D. dissertation of Mingda She.

0006-3495/97/08/1042/14 $2.00

ration by Ca^{2+}. On this basis a computer model has been proposed for the 4-Ca state of TnC that predicts significant and large-scale rearrangements of helices B and C relative to helices N, A, and D (Herzberg et al., 1986; Strynadka and James, 1989). These putative structural changes may play a role in calcium regulation.

TnC from fast chicken skeletal muscle contains no tyrosine or tryptophan, and this property allows introduction of a single tryptophan (Pearlstone et al., 1992a) or tyrosine (Pearlstone et al., 1992b) as an optical probe for the conformations of different regions of the protein and to investigate structure/function relationships. We have recently constructed a series of single-tryptophan TnC mutants by site-directed mutagenesis and used them in a preliminary energy transfer study (She et al., 1995) to monitor global conformational changes induced by the binding of activator Ca^{2+} to the regulatory sites. In the present work, we report time-resolved fluorescence properties of these mutants, which contain single tryptophan residues at positions 22, 52, and 90 and single cysteine residues at other positions, and discuss the effects of activator Ca^{2+} on both local and global conformations of TnC.

MATERIALS AND METHODS

Generation and preparation of TnC mutants

The construction of the expression vector and the production of TnC mutants by site-directed mutagenesis has been described (She et al., 1997). Briefly, a cDNA encoding full-length TnC of chicken fast skeletal muscle and the pT7-7 expression vector were used. The recombinant proteins were overexpressed in *Escherichia coli* BL21(DE3), and mutations in various positions were directed by synthesized oligonucleotides containing the mutated basepairs. Polymerase chain reaction (PCR) was used to generate the cDNA segments containing the specified basepair changes, and these PCR fragments were treated with appropriate restriction enzymes and inserted into the corresponding sites of digested expression plasmid of wild-type or mutant TnC. The mutations were confirmed by chain-termination DNA sequencing of the entire primary region.

Steady-state fluorescence spectroscopy

Steady-state fluorescence measurements were made on an SLM 8000C spectrofluorometer at 20.0 ± 0.1°C in a basic buffer system containing 0.1 M KCl, 25 mM MOPS at pH 7.2, and 1 mM EGTA, unless stated otherwise. When Mg^{2+} was present, it was 2 mM $MgCl_2$. When Ca^{2+} was present, the free Ca^{2+} concentration was controlled by EGTA and calculated by using Fabiato's program (Fabiato, 1988) and known stability constants of the chelator for proton, Ca^{2+}, and Mg^{2+}. Unless stated otherwise, the free Ca^{2+} concentration was adjusted to 1 mM. Fluorescence emission spectra were corrected for the variation of the detector system response with wavelength. Quantum yields of tryptophan in TnC mutants were determined by the comparative method (Parker and Rees, 1960), using L-tryptophan as the standard. A value of 0.14 was used as the quantum yield of the amino acid (Valeur and Weber, 1977). Quenching of tryptophan fluorescence intensity was determined by the addition of aliquots of an 8 M solution with λ_{ex} = 295 nm and λ_{em} at the peak of the emission spectrum. A correction was made for inner filter effects due to the absorbance of acrylamide at the excitation wavelength. The quenching data were fitted to a modified Stern-Volmer equation:

$$\frac{F_o}{F} = (1 + K_{SV}[Q])\exp(V[Q]) \qquad (1)$$

where F_o and F are the fluorescence intensities in the absence and presence of quencher, respectively; $[Q]$ is the molar quencher concentration; K_{SV} is the Stern-Volmer dynamic quenching constant; and V is the static quenching constant.

Time-resolved fluorescence measurement

Tryptophan intensity decay and anisotropy decay of TnC mutants were measured in the basic buffer system at 23°C on a PRA photon-counting system (model 3000) with a rhodamine 6G dye laser as the excitation source. The dye laser was synchronously pumped by a mode-locked argon ion laser (Spectra-Physics model 171) at 514.5 nm. The mode-locker operated at 41 MHz, and the cavity-dumped dye laser was set at 4 MHz and provided a train of light pulses with a full width at half-maximum = 15 ps. The output from the dye laser was frequency-doubled to 295 nm by an angle-tuned KDP crystal (Spectra-Physics model 390) to generate uv picosecond pulses, the frequency of which was tunable from 280 to 310 nm. The laser intensity was attenuated by neutral density filters such that the emission rate from samples were reduced to <3 kHz to avoid photon pile-up. The PM tube was a Hamamatsu R955, and the photon counting system had a response time of 500–600 ps in half-width. For lifetime measurements, the excitation polarizer was set at the vertical direction and the emission polarizer was oriented at the magic angle (54.7° from the horizontal). The emission was detected at a right angle to the excitation beam, and the emission wavelengths were selected with a 4-nm band pass monochromator (Instruments SA, Inc.). Cutoff filters (Schott WG 305 or WG 320) were used to eliminate scattered uv light. Decay curves were collected into 1024 channels of a multichannel analyzer at a resolution of 20 ps/channel until 10^4 photon counts were collected in the peak channel.

The intensity decay data were fitted to a sum of exponential terms (Grinvald and Steinberg, 1974) by using a least-squares reconvolution procedure:

$$F(t) = \sum_{i=1} \alpha_i \exp(-t/\tau_i) \qquad (2)$$

where τ_i are the lifetimes and α_i are the corresponding fractional amplitudes. The goodness of a fit was assessed by the weighted residuals, the autocorrelation function of the residuals, the reduced chi-squares ratio, and the Durbin-Watson number (D-W) as was previously described (Liao et al., 1992). Anisotropy decays were determined by using vertically polarized excitation and measuring the emitted light polarized in the vertical $[F_{\parallel}(t)]$ and horizontal $[F_{\perp}(t)]$ directions. The two polarized decay components were alternately collected into 1024 channels at a resolution of 20 ps/channel in a series of 500-s cycles to minimize fluctuation effects of both the lasers and electronics. Typically, 50,000 photons were collected in the peak channel for $F_{\parallel}(t)$, and the $F_{\perp}(t)$ component was counted for the same length of time as for $F_{\parallel}(t)$. The time-dependent anisotropy $r(t)$ was calculated from the difference and sum curves obtained from the two polarized components:

$$r(t) = \frac{F_{\parallel}(t) - GF_{\perp}(t)}{F_{\parallel}(t) + 2GF_{\perp}(t)} \qquad (3)$$

The G-factor, which corrects for optical differences in the collection of the two polarized decay components, was determined by using horizontally polarized excitation to collect vertically and horizontally polarized emission decay data. The ratio of the integrated intensities of the vertical and horizontal decay components was used as the G-factor. The calculated anisotropy data were fitted to a sum of exponential terms:

$$r(t) = r_o \sum_i g_i \exp(-t/\phi_i) \qquad (4)$$

where ϕ_i are the rotational correlation times with fractional amplitudes g_i, and r_o is the limiting anisotropy at zero time. For a two-component fit, the total anisotropy r_o is given by $r_o = g_1 r_o + g_2 r_o$ with $g_1 + g_2 = 1.0$.

Decay-associated emission spectra (DAS) were constructed from the steady-state emission spectra and intensity decay data (Wahl and Auchet, 1972)

$$F_i(\lambda) = \frac{F(\lambda)\alpha_i(\lambda)\tau_i(\lambda)}{\sum_j [\alpha_j(\lambda)\tau_j(\lambda)]} \quad (5)$$

where $F_i(\lambda)$ is the fluorescence intensity associated to the ith decay component with decay time τ_i at the wavelength λ. $F(\lambda)$ is the intensity of the steady-state spectrum at λ, and α_i are the preexponential amplitudes associated with the lifetimes τ_i.

RESULTS

Tryptophan-containing TnC mutants

Three single mutants (F22W, N52W, and A90W) and three triple mutants were studied in this work. The triple mutants were F22W/C101L/N52C (M-1), N52W/C101L/F13C (M-2), and A90W/C101L/N52C (M-3), and they each had a single tryptophan at positions 22, 52, and 90, respectively. The other two substitutions in the triple mutants were made to replace the single Cys-101 by leucine and place a single cysteine at a specific location at the N-terminal half of TnC. These substitutions yielded mutants that contained a single tryptophan and a single cysteine and allowed covalent attachment of an energy acceptor probe to the sulfhydryl group for fluorescence resonance energy transfer studies, using the tryptophan as an energy donor. The replacement of Cys-101 was expected to have a minimum of structural and functional effects because the residue in the homologous position in cardiac muscle TnC is leucine. As will be shown below, the properties of the single tryptophan in F22W and the corresponding triple mutant were very similar, indicating that the two additional mutations had negligible effects on Trp-22. Similar results were obtained for the other two tryptophan residues. We present in this report the time-resolved fluorescence properties of tryptophan in F22W and the three triple mutants. Fig. 1 shows the three residues in the TnC structure that were replaced by tryptophan.

Quenching of tryptophan fluorescence by acrylamide

To characterize the local environments of the tryptophans in the TnC mutants, a series of experiments were carried out to determine the extent of quenching of their steady-state fluorescence by acrylamide. The Stern-Volmer plots are shown in Fig. 2. The plots showed a concave upward curvature regardless of whether Ca^{2+} was absent or present and were analyzed by Eq. 1 to obtain the Stern-Volmer dynamic quenching constant (K_{SV}) and the static quenching constant (V). These results are given in Table 1, together with other relevant steady-state fluorescence parameters.

The steady-state fluorescence properties (Q and λ_{em}) of Trp-22 in F22W were indistinguishable from those of the triple mutant M-1 (Table 1). In the presence of Mg^{2+}, only

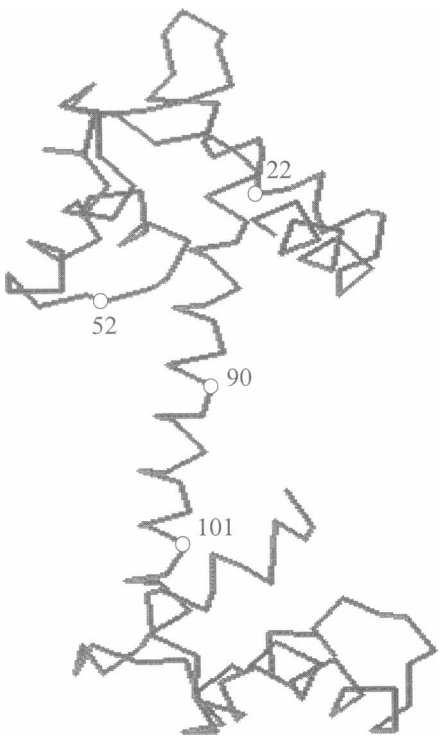

FIGURE 1. Diagram showing the crystal structure of TnC and the three residues that were replaced by tryptophan. These are residue 22, 52, and 90. Also shown is the position of Cys-101, which was replaced by leucine.

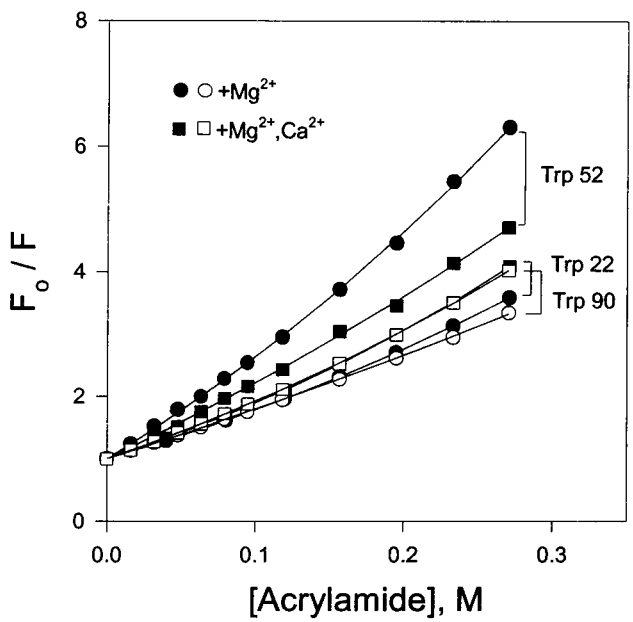

FIGURE 2 Stern-Volmer plots of acrylamide quenching of single tryptophan in positions 22, 52, and 90 of TnC mutants. The measurements were made in the presence of Mg^{2+} or in the presence of Mg^{2+} + Ca^{2+} with mutant M-1 for Trp-22, M-2 for Trp-52, and M-3 for Trp-90. Protein concentration was ~5 μM in the basic buffer system (see text). Circles, in the presence of 2 mM Mg^{2+}; squares, in the presence of 2 mM Mg^{2+} + 2 mM free Ca^{2+}. The quenching parameters are listed in Table 1.

TABLE 1 Fluorescence parameters of TnC mutants containing single tryptophan

Trp/mutant	Ligand	Q	λ_{em} (nm)	K_{SV} (M^{-1})	V (M^{-1})	$k_q \times 10^{-9}$ ($M^{-1}\ s^{-1}$)	$k_r \times 10^{-7}$ (s^{-1})	$k_{nr} \times 10^{-7}$ (s^{-1})
22(F22W)	Mg^{2+}	0.33	331	5.81	1.34	1.02	5.8	11.7
	Ca^{2+}	0.25	332	5.28	1.79	1.12	5.3	15.8
22(M-1)	Mg^{2+}	0.33	331	5.70	1.25	1.00	5.3	15.8
	Ca^{2+}	0.25	332	5.66	1.74	1.20	5.3	15.8
52(M-2)	Mg^{2+}	0.13	351	14.3	0.78	3.49	3.1	21.0
	Ca^{2+}	0.11	351	10.4	1.00	2.60	2.7	22.2
90(M-3)	Mg^{2+}	0.12	345	7.21	0.30	1.76	3.6	28.9
	Ca^{2+}	0.17	343	6.85	1.15	1.29	4.1	19.8

All parameters were determined in the basic buffer system containing 2 mM $MgCl_2$. When Ca^{2+} was present, the system also contained 1 mM free Ca^{2+} in addition to 2 mM $MgCl_2$. Quantum yield Q and λ_{em} are taken from She et al. (1997). The Stern-Volmer dynamic quenching constant (K_{SV}) and the static quenching constant (V) were obtained from acrylamide quenching measurements. The dynamic bimolecular quenching constant (k_q) was calculated from $k_q = K_{SV}/\langle\tau\rangle$, where $\langle\tau\rangle$ is the intensity-weighted mean fluorescence lifetime calculated from $\langle\tau\rangle = \Sigma\alpha_i(\tau_i)^2/\Sigma(\alpha_i\tau_i)$. The radiative decay rate k_r was calculated from $k_r = Q/(\Sigma\alpha_i\tau_i)$, and the nonradiative decay rate was calculated from $k_{nr} = k_r/Q - k_r$ (Werner and Foster, 1979), where Q is the quantum yield. These rate constants were calculated from decay data obtained at 350 nm.

the two high-affinity Ca/Mg sites were occupied and the two low-affinity regulatory sites were unoccupied. Saturation of the regulatory sites by adding Ca^{2+} induced a small increase in the apparent static quenching and a small decrease in K_{SV}. The value of the bimolecular quenching rate ($k_q = 1.02 \times 10^9\ M^{-1}\ s^{-1}$) indicated that, in the absence of bound activator Ca^{2+}, Trp-22 was substantially protected from collision with solvent molecules (Eftink and Ghiron, 1976). In the presence of bound activator Ca^{2+}, k_q was slightly larger, indicating the tryptophan to be in an environment slightly more accessible to collisional quenching but still substantially protected. This is in agreement with a 24% decrease in quantum yield and a small red spectral shift.

Trp-90 in M-3 was sufficiently buried in the presence of Mg^{2+}, with a k_q of $1.76 \times 10^9\ M^{-1}\ s^{-1}$. Saturation of the two regulatory sites by Ca^{2+} increased the apparent static quenching and reduced k_q. The decrease in k_q is consistent with an increase in quantum yield and a blue-shift of the spectrum, indicating an environment slightly less accessible to solvent.

The quantum yield of Trp-52 in the mutant M-2 was more than a factor of 2 smaller than that of Trp-22. In the absence of bound activator Ca^{2+}, the value of k_q was high, approaching the value ($4 \times 10^9\ M^{-1}\ s^{-1}$) expected of a fully exposed tryptophan in protein (Eftink and Ghiron, 1976). Upon addition of Ca^{2+}, the exposure of Trp-52 was reduced, but still substantially exposed ($k_q = 2.60 \times 10^9\ M^{-1}\ s^{-1}$). The apparent Ca^{2+}-induced protection from solvent was not accompanied by a detectable spectral shift, and the small decrease in quantum yield was in the opposite direction expected for increased protection from solvent accessibility.

Intensity decay of Trp-22 in TnC mutants

The intensity decays of the single-tryptophan TnC mutants were measured and analyzed by a sum of exponential terms. The decays of Trp-22 in F22W determined in the presence of EGTA and in the presence of Mg^{2+} (2-Mg state) were essentially identical and adequately fitted with a single exponential function. A typical decay of F22W determined in the presence of Mg^{2+} is shown in Fig. 3 *a*. The best fitted single lifetime was 5.65 ns. Using the same optical conditions, we determined that the decay of *N*-acetyl-L-tryptophanamide (NATA) at pH 7.5 was monoexponential with a single lifetime of 2.85 ± 0.03 ns ($\chi^2_R = 1.08$, D-W = 2.10), in excellent agreement with a recent report (Davis et al., 1994). This result served to validate the observed monoexponential decay of F22W (Fig. 3 *a*). The monoexponential decay pattern was independent of emission wavelength (310–400 nm), and the average of the recovered single lifetimes determined at 10-nm intervals was 5.68 ± 0.04 ns. These results suggested that Trp-22 in the 2-Mg state of F22W was likely in a very homogeneous microenvironment. Listed in Table 2 are the lifetimes for three selected wavelengths.

Fig. 3 *b* shows the decay of F22W determined at 330 nm in the presence of both Mg^{2+} and Ca^{2+}. In this experiment, Ca^{2+} was added to the sample from Fig. 3 *a* so that Mg^{2+} already bound to the high-affinity Ca/Mg sites was displaced by Ca^{2+}, and the low-affinity Ca^{2+}-specific sites were saturated with Ca^{2+} (4-Ca state). It is clear that the decay could not be fitted to a monoexponential function, but could be adequately fitted to a biexponential function, yielding $\tau_1 = 4.91$ ns and $\tau_2 = 2.27$ ns, with fractional amplitudes of 0.82 and 0.18 for the long and short components, respectively. The mean value (intensity weighted) of the two lifetimes was 4.67 ns, substantially smaller than the single lifetime determined in the absence of bound Ca^{2+} in the N-domain. None of the decays obtained at other wavelengths over the range of 310–400 nm could be fitted to a monoexponential function, but they all could be fitted satisfactorily with two exponential terms. The lifetimes recovered at three selected wavelengths for F22W in the presence of Ca^{2+} are given in Table 2. A remarkable feature of the decay is that both τ_1 and τ_2 increased with increasing emission wavelength, with the amplitude associated with τ_1

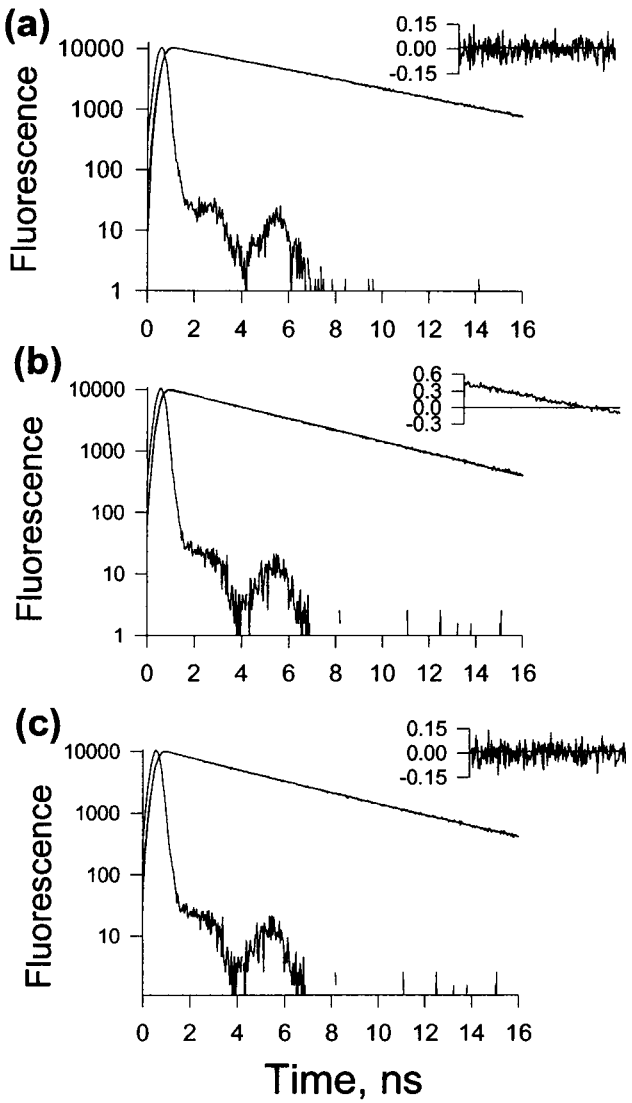

FIGURE 3 Representative plots of the fluorescence intensity decay of Trp-22 in F22W determined with ~5 μM protein. (*a*) In the presence of 2 mM $MgCl_2$; under this condition, the two Ca/Mg sites in the C-terminal domain were occupied by Mg^{2+} and the two Ca^{2+}-specific, regulatory sites in the N-terminal domain were vacant. The decay was fitted to a single exponential function with τ = 5.65 ns, χ^2_R = 1.05, and D-W = 2.10. The inset at the upper right-hand corner is the autocorrelation function of the residuals. The sharp peak on the left is the lamp profile. (*b*) In the presence of 2 mM Mg^{2+} + 1 mM free Ca^{2+}. Under these conditions, the two regulatory sites were saturated by Ca^{2+}. The decay was fitted to a monoexponential function, yielding τ = 4.61 ± 0.01 ns, χ^2_R = 2.13, and D-W = 1.00. (*c*) The same decay curve shown in (*b*) was fitted with a biexponential function: τ_1 = 4.91 ± 0.03 ns, τ_2 = 2.27 ± 0.15 ns, α_1 = 0.82 ± 0.02, α_2 = 0.18 ± 0.02; χ^2_R = 1.01 and D-W = 2.15. The emission was monitored at 330 nm. Other conditions are given in the text.

decreasing from 0.76 at 310 nm to 0.43 at 400 nm. Fig. 4 *a* shows the dependence of the two Ca^{2+}-mediated lifetimes on emission wavelength, and Fig. 4 *b* shows the corresponding changes in the amplitudes. At each wavelength, the mean lifetime in the presence of Ca^{2+} was ~1 ns shorter than in its absence. These changes resulted from Ca^{2+} binding to all four sites. Since the decay was monoexponential when the two high-affinity sites were occupied by Mg^{2+}, the Ca^{2+}-induced biexponential decays reflected the binding of Ca^{2+} to the two Ca^{2+}-specific regulatory sites.

The decay pattern of Trp-22 in the triple mutant M-1 was indistinguishable from that in the single mutant F22W, when determined in the presence of Mg^{2+}, throughout the entire wavelength range studied. The results for three selected wavelengths are included in Table 2. In the presence of Mg^{2+} plus Ca^{2+}, the decays of Trp-22 in the mutant M-1 were biexponential throughout the entire wavelength range studied, and the weighted mean lifetimes were very similar to the values obtained with F22W (Table 2). These results and the steady-state results suggested that the two additional amino acid substitutions in positions 52 and 101 had a minimum of effects on the emission properties of Trp-22.

Intensity decays of Trp-52

The decay of Trp-52 in mutant M-2 measured in the presence of Mg^{2+} could not be fitted with a single exponential function. Fig. 5 *a* shows a typical biexponential fit to the decay curve of M-2. In the presence of Mg^{2+} plus Ca^{2+}, three exponential terms were required for a satisfactory fit (Fig. 5 *b*). The lifetimes obtained at three selected wavelengths for M-2 are given in Table 2. In the presence of Mg^{2+}, τ_1 was relatively insensitive to emission wavelength, but τ_2 increased by 1 ns from the blue edge to the red edge of the spectrum. The fractional amplitude α_1 increased with emission wavelength up to ~350 nm, then remained relatively constant into the red edge of the spectrum. These results are depicted in Fig. 6, *a* and *b*. Unlike the environment of Trp-22, these results suggested that Trp-52 in the 2-Mg state of M-2 was likely in a heterogeneous microenvironment. In the presence Ca^{2+}, τ_1 increased by ~2 ns with increasing wavelength, whereas the two shorter components were less sensitive to wavelength (Fig. 6 *c*). The amplitudes of τ_2 and τ_3 changed in opposite directions, and the amplitude of the longest lifetime was not very sensitive to wavelength (Fig. 6 *d*). Ca^{2+} induced a small or negligible reduction (<0.5 ns) in the mean lifetime at each wavelength. This Ca^{2+}-mediated change was in the same direction as that observed with F22W and M-1, although the magnitude of the change was considerably smaller.

Intensity decay of Trp-90

The decay of Trp-90 in M-3 was more complex than that of tryptophan at the other two positions. In the presence of Mg^{2+}, the decay could be adequately described only with a triexponential function (Table 2) in the range of 310–350 nm. Above 350 nm, the decays could be fitted with either a biexponential or a triexponential function. The mean lifetimes at each wavelength from the two different fits differed by only 0.1–0.2 ns, and this small difference was not considered significant. Thus, the decay of M-3 was subsequently analyzed by three exponential terms, yielding three

TABLE 2 Representative multiple exponential analysis of the fluorescence decays of TnC mutants containing single tryptophan

Mutant/ligand		λ_{em} (nm)	τ_1 (α_1) (ns)	τ_2 (α_2) (ns)	τ_3 (α_3) (ns)	$\langle\tau\rangle$ (ns)	χ^2_R
F22W	Mg^{2+}	310	5.68			5.68	1.20
		330	5.65			5.65	1.10
		400	5.72			5.72	1.03
	Ca^{2+}	310	4.88 (0.76)	1.89 (0.25)		4.54	1.09
		330	4.91 (0.82)	2.27 (0.18)		4.67	1.19
		400	5.75 (0.43)	3.50 (0.57)		4.92	1.15
M-1	Mg^{2+}	310	5.61			5.61	1.07
		330	5.67			5.67	1.20
		400	5.77			5.77	1.12
	Ca^{2+}	310	4.88 (0.79)	1.82 (0.21)		4.61	1.21
		330	5.18 (0.67)	3.08 (0.33)		4.71	1.10
		400	7.92 (0.07)	4.46 (0.93)		4.87	1.17
M-2	Mg^{2+}	310	4.15 (0.58)	0.95 (0.42)		3.70	1.30
		330	4.31 (0.70)	1.28 (0.30)		3.97	1.26
		400	4.51 (0.75)	1.95 (0.25)		4.19	1.10
	Ca^{2+}	310	5.00 (0.18)	2.22 (0.39)	0.46 (0.44)	3.31	1.01
		330	5.99 (0.17)	2.83 (0.51)	0.65 (0.32)	3.87	1.07
		400	6.95 (0.14)	3.17 (0.66)	0.83 (0.20)	4.19	1.10
M-3	Mg^{2+}	320	5.41 (0.20)	2.43 (0.38)	0.71 (0.42)	3.63	0.95
		370	5.82 (0.29)	2.81 (0.47)	1.02 (0.24)	4.25	1.01
		400	10.4 (0.03)	4.41 (0.59)	1.54 (0.37)	4.51	1.18
	Ca^{2+}	320	5.45 (0.51)	1.33 (0.49)		4.67	1.56
		370	5.88 (0.64)	1.88 (0.36)		5.26	1.12
		400	6.00 (0.65)	2.20 (0.35)		5.37	1.19

The measurements were carried out with samples containing 3–5 μM protein. See Table 1 for other conditions. The fractional amplitudes (α_i) associated with the lifetimes τ_i are given in parentheses. The intensity-weighted mean lifetime $\langle\tau\rangle$ was calculated as shown in Table 1. In addition to the reduced chi-squares ratio (χ^2_R), other statistical criteria were also used to judge the goodness of fit of each decay curve (see text). The standard errors obtained from the least-squares fitting were in the range of 0.03–0.07 ns for τ_i and 0.01–0.07 for α_i.

lifetimes in the range of ~5 ns, 2–3 ns, and 0.6–1.4 ns with samples containing Mg^{2+}. The three resolved lifetimes were sufficiently separated and the ratio of τ_i/τ_{i+1} was generally ≥2. This suggests that the resolution of the three lifetimes was not problematic. The goodness of fit was supported by several statistical criteria. With increasing wavelength, all three lifetimes increased (Fig. 7 *a*). A plot of the three amplitudes versus wavelength obtained in the presence of Mg^{2+} showed considerable scatter (data not shown). In the presence of Mg^{2+} plus Ca^{2+}, the decay was adequately fitted with a biexponential function, and the two lifetimes also increased with increasing wavelength (Fig. 7 *b*). The amplitudes of the long lifetime increased from 0.51 at 310 nm to 0.65 at 400 nm in a manner similar to M-2 (Fig. 6 *b*). Ca^{2+} induced a 1-ns increase in the mean lifetime across the emission band. This change in $\langle\tau\rangle$ was in a direction opposite to that obtained with Trp-22 and Trp-52.

Anisotropy decays of tryptophan in TnC mutants

The anisotropy decays of the single tryptophan in TnC mutants were determined in the presence of Mg^{2+} and Mg^{2+} + Ca^{2+}. All decay curves were biphasic and could be adequately fitted to a biexponential function. Fig. 8 *a* shows a representative anisotropy decay plot for F22W determined in the presence of Mg^{2+}. The long rotational correlation time (ϕ_1) was 8.1 ns, and the short correlation time (ϕ_2) was 0.8 ns. The value of ϕ_1 increased to 10.1 ns and the value of ϕ_2 increased to 1.5 ns upon addition of Ca^{2+} (Fig. 8 *b*). Essentially identical rotational correlation times were obtained for F22W and M-1. The anisotropy parameters of these proteins and M-2 and M-3 are listed in Table 3. The zero-time anisotropy values were smaller than the value expected of indole similarly excited (Valeur and Weber, 1977). The smaller observed values could be due to depolarization arising from fast side-chain motions that were not resolved in the present experiments. The cone semiangle (θ) calculated from these data were lower limits. The values of the long rotational correlation time obtained in the presence of Mg^{2+} plus Ca^{2+} for M-3 were essentially the same as the corresponding values observed with M-1. The values of this long correlation time of M-2, however, were significantly smaller than those of M-1 and M-3. The calculated cone semiangle of the tryptophan side chain (θ) in F22W and M-1 was significantly smaller than that for M-2 and M-3. Ca^{2+} had no apparent effect on θ for F22W and M-1, but had an effect for M-2 and M-3. With M-2 Ca^{2+} increased the semiangle, whereas with M-3 it decreased this angle. These different Ca^{2+} effects were related to the local structure of the three tryptophan residues.

DISCUSSION

We have studied the fluorescence decay of a single mutant and three triple mutants of skeletal muscle TnC. These mutants each contain a single tryptophan residue located in

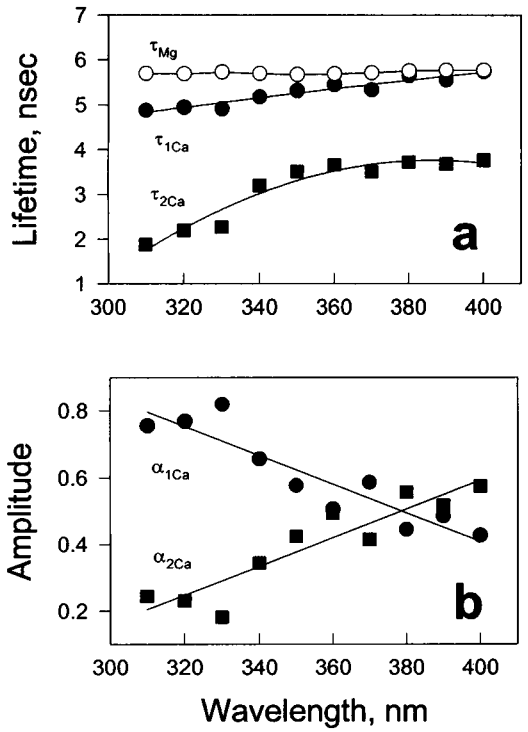

FIGURE 4 The dependence of the lifetimes and amplitudes on emission wavelength for F22W determined in the presence of Mg^{2+} and Mg^{2+} + Ca^{2+}. (*a*) Lifetime versus wavelength. Open circle, the single lifetime determined in the presence of Mg^{2+}. Closed circle and square, the two lifetimes determined in the presence of Mg^{2+} + Ca^{2+}. (*b*) Fractional amplitudes associated with τ_1 (*closed circle*) and τ_2 (*closed square*) determined in the presence of Mg^{2+} + Ca^{2+}. These data were collected under the same conditions given in the legend to Fig. 3. The lines in the figures were drawn arbitrarily through the points to indicate the direction of changes of the parameters.

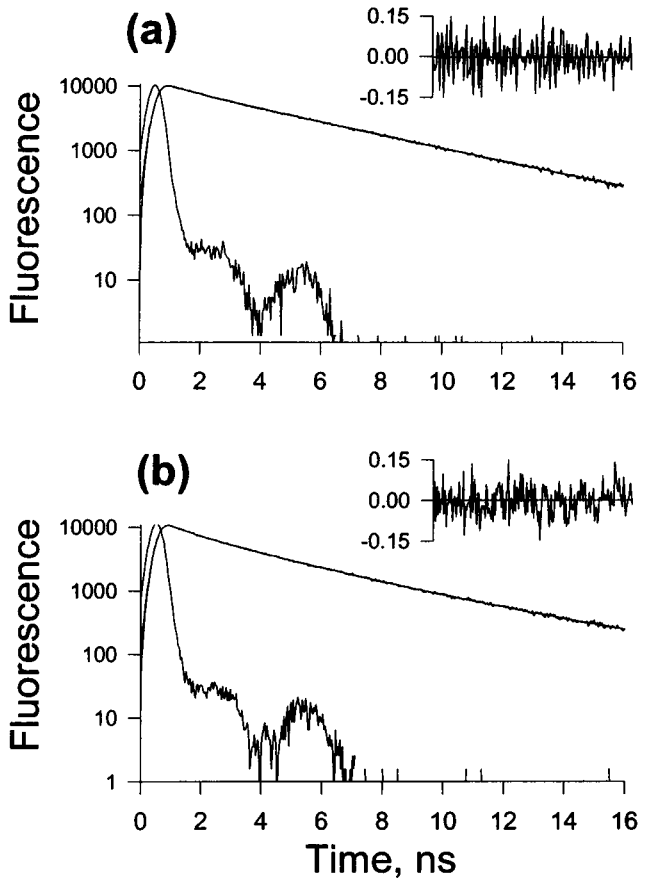

FIGURE 5 Representative intensity decay curves of Trp-52 in mutant M-2 determined at 355 nm. (*a*) The decay was determined in the presence of Mg^{2+}, and the data were fitted to a biexponential function, yielding τ_1 = 4.44 ± 0.02 ns, τ_2 = 1.55 ± 0.08 ns, α_1 = 0.76 ± 0.01, α_2 = 0.24 ± 0.01; χ^2_R = 1.16, D-W = 2.05. (*b*) The decay was collected in the presence of Mg^{2+} + Ca^{2+} and analyzed by a triexponential function. τ_1 = 6.39 ± 0.28 ns, τ_2 = 3.02 ± 0.12 ns, τ_3 = 0.75 ± 0.06 ns, α_1 = 0.16 ± 0.03, α_2 = 0.59 ± 0.02, α_3 = 0.25 ± 0.01; χ^2_R = 0.99, D-W = 1.96. Other experimental conditions were the same as given in the legend to Fig. 3.

the regulatory N-domain. The tryptophan residue was introduced as an optical probe of the conformation of the regulatory domain in response to the binding of activator Ca^{2+} at the two regulatory sites. The other two amino acid substitutions were made to allow specific labeling of a single cysteine residue with an extrinsic probe serving as a donor/acceptor pair with tryptophan in energy transfer studies (She et al., 1995). Circular dichroism, energy minimization, and molecular graphics suggest no gross structural alteration in the N-domain of TnC due to the mutations, including the introduction of a single tryptophan at three positions (22, 52, and 90) (She et al., 1997). The mutants retain full functional activities, including Ca^{2+} binding and regulation of myofibrillar ATPase activity.

The decay properties of Trp-22 in the single mutant F22W and the triple mutant M-1 are very similar, indicating that the two additional point mutations in M-1 within the N-terminal domain do not affect the local environment of Trp-22 to any appreciable extent. The single lifetime of F22W in the absence of bound Ca^{2+} at the two regulatory sites suggests a homogeneous microenvironment in which the side chain of the residue exists in a single conformation. The very high quantum yield (0.33) and long lifetime (>5 ns) could result from either a significant alteration of the electronic structure of the singlet state of Trp-22 or reduction of nonradiative decay rates as compared with an isolated indole ring. The radiative decay rate (k_r) is estimated to be $5.8 \times 10^7\ s^{-1}$ for F22W (Table 1), in good agreement with that of $5 \times 10^7\ s^{-1}$ for NATA (Werner and Foster, 1979). On the other hand, the nonradiative decay rate for the mutant ($k_{nr} = 11.7 \times 10^7\ s^{-1}$) is about a factor of 3 smaller than that for NATA ($31 \times 10^7\ s^{-1}$), indicating that the reduced nonradiative rate is likely responsible for the observed high quantum yield. This conclusion is consistent with the 20-nm blue-shift of the emission spectrum relative to tryptophan in water at neutral pH (351 nm as measured with our system). The upward curvature in the Stern-Volmer quenching plots is traditionally interpreted in terms of an apparent static quenching with a static quenching constant V (Eq. 2). This constant contains contributions from 1) transient quenching as described by the time-dependent Smoluchowski diffusion equation, and 2) true static

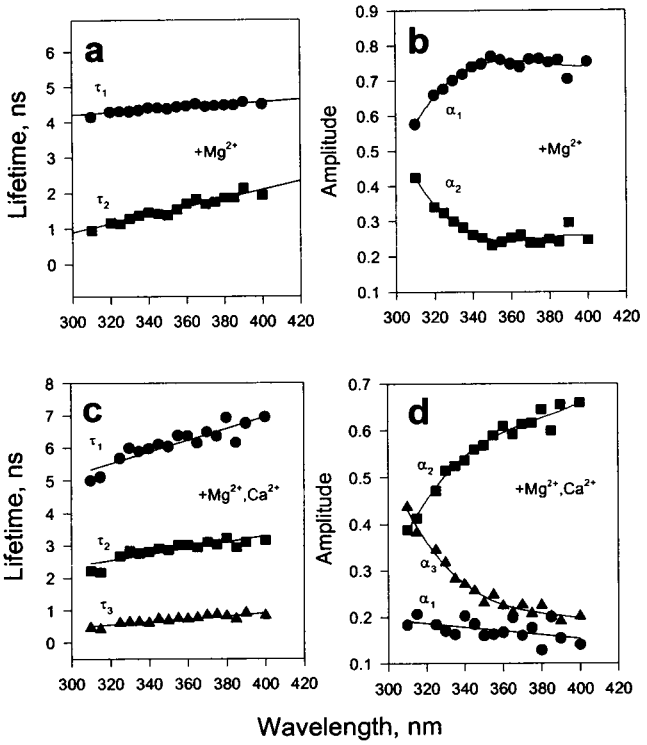

FIGURE 6 The dependence of lifetimes and the associated amplitudes on emission wavelength for M-2. (*a*) The two recovered lifetimes determined in the presence of Mg^{2+}, and (*b*) the fractional amplitudes associated with the two lifetimes shown in (*a*). Circles, the long decay component (τ_1 and α_1); squares, the short component (τ_2 and α_2). (*c*) The three lifetimes determined in the presence of Mg^{2+} + Ca^{2+}; (*d*) the corresponding fractional amplitudes associated with the lifetimes shown in (*c*). Circles, τ_1 and α_1; squares, τ_2 and α_2; triangles, τ_3 and α_3. Conditions were the same as for Fig. 5.

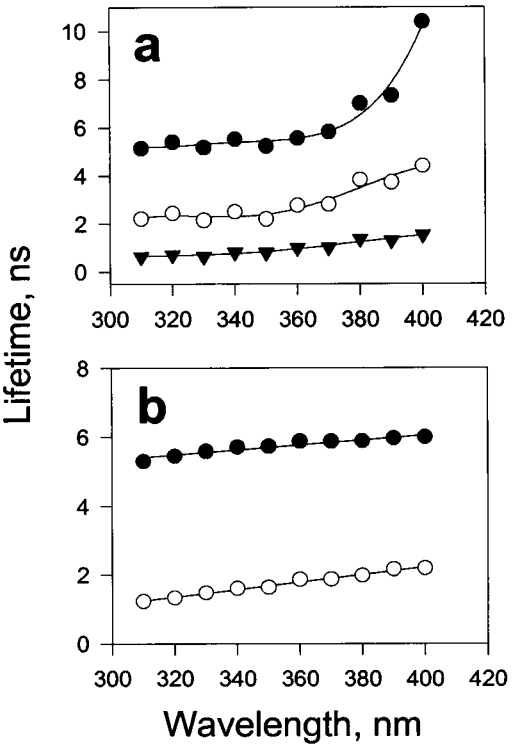

FIGURE 7 The variation of the lifetimes of Trp-90 in mutant M-3 as a function of emission wavelength in the presence of Mg^{2+} (*a*) and in the presence of Mg^{2+} + Ca^{2+} (*b*).

quenching in which a chemically distinct ground-state, nonfluorescent complex is formed before excitation. Transient quenching alone is sufficient to cause an upward curvature without invoking static quenching (Eftink, 1991). Regardless of the origin of the observed upward curvature, the small value of the bimolecular collisional quenching constant (k_q = 1.02 × 10^9 M^{-1} s^{-1}) obtained from the initial slope of the plot is a valid measure of solvent accessibility and indicates that the indole in F22W is substantially buried and protected from solvent. The x-ray structure of the 2-Ca state of TnC shows that Phe-22 in native TnC is indeed partially buried and not readily accessible to solvent. Other studies suggest that replacement of Phe-22 by Trp would retain similar side-chain packing as in the native structure, and Trp-22 in the mutant would be similarly inaccessible to solvent (She et al., 1997).

In the presence of bound activator Ca^{2+} at the regulatory sites, the radiative decay rate (k_r = 5.3 × 10^7 s^{-1}) is little changed, but the nonradiative rate increases by 35%. The Trp-22 decay becomes biexponential with the mean lifetime smaller than the single lifetime determined in the 2-Mg state. This decrease in lifetime is manifested in a decrease in quantum yield and a small, but reproducible, red spectral shift and a small increase in k_q. Taken together, these results suggest that Trp-22 in the 4-Ca state becomes more exposed to solvent and is in an environment in which nonradiative decay processes become important in deactivation of the excited tryptophan. This conclusion is consistent with the modeled structure of the 4-Ca state of TnC, which suggests that the solvent-accessible surface of Phe-22 increases from 4.1 $Å^2$ in the 2-Ca state to 20.1 $Å^2$ in the 4-Ca state (Herzberg et al., 1986; Stryndka and James, 1989).

The single lifetime of F22W in the 2-Mg state is independent of emission wavelength, but the mean lifetime in the 4-Ca state has a wavelength dependence. We consider two possibilities for this dependence. One is related to excited-state reactions involving the tryptophan, and the other is ground-state heterogeneity. Early studies showed that solvent reorientation around an excited fluorophore can result in an increase in lifetime with increasing wavelength (Bakhshiev et al., 1966; Ware et al., 1971). Solvation of the excited-state may lead to emission from a large number of emitting species. If the characteristic time τ_R of this dipolar reorientation is comparable to the fluorescence decay time τ_F, deviation from monoexponential decay can be expected (DeToma et al., 1976). Under these conditions, emission can occur from a wide range of fluorophores that have relaxed to different extents. The unrelaxed and partially relaxed species emit with higher energy at the blue edge of the spectrum, and relaxed species emit with smaller energy in the red edge of the spectrum. The fraction of relaxed

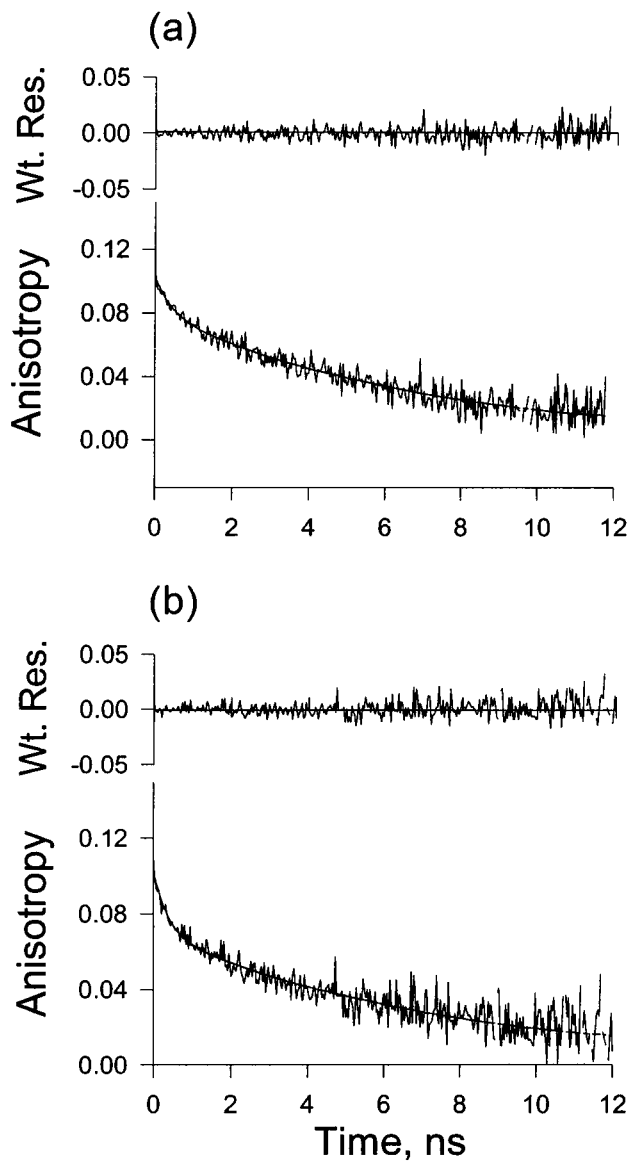

FIGURE 8 Representative anisotropy decay plots of F22W. (*a*) The decay was determined in the presence of Mg^{2+}: $\phi_1 = 8.31 \pm 0.25$ ns, $\phi_2 = 0.80 \pm 0.30$ ns, $r_1 = 0.120 \pm 0.003$, $r_2 = 0.023 \pm 0.005$, $r_o = 0.143 \pm 0.008$; $\chi^2_R = 1.27$. (*b*) Decay determined in the presence of Mg^{2+} + Ca^{2+}: $\theta_1 = 11.59 \pm 0.45$ ns, $\theta_2 = 1.16 \pm 0.33$ ns, $r_1 = 0.119 \pm 0.003$, $r_2 = 0.022 \pm 0.003$, $r_o = 0.141 \pm 0.006$; $\chi^2_R = 1.28$. The panels across the top of the figures are the weighted residuals of the fits. The measurements were carried out with ~5 μM protein, and the emission was detected with a Schott WG 320 cutoff filter.

fluorophores increases with increasing wavelength, leading to longer decay times. The mean lifetime is expected to increase with increasing wavelength (Lakowicz and Cherek, 1980). This is what was observed for the decay of F22W in the 4-Ca state. On the other hand, the lack of a wavelength dependence for the single lifetime determined in the 2-Mg state suggests the emission in this state to occur from either unrelaxed or relaxed tryptophan residues (i.e., $\tau_R \gg \tau_F$ or $\tau_R \ll \tau_F$). In the absence of bound Ca^{2+} at the regulatory sites, the molecular graphics show the indole ring of Trp-22 to be within 3–4 Å from a number of hydrophobic side chains including Met-86, Leu-79, Met-18, Leu-49, and Met-82. There is a potential hydrogen bond (3.98 Å) between the indole N—H and the oxygen of uncoordinated carboxylate of Glu-21. In the modeled 4-Ca state, the indole ring appears to be rotated by ~90° about the C_β—C_γ bond and is still within van der Waals contacts with the hydrophobic side chains. The indole N—H now is away from the Glu-21 carboxylate group. In this Ca^{2+}-induced conformation, the tryptophan side chain appears to be in a very similar constrained environment, although the edge of the indole ring is slightly more accessible to solvent. It is difficult to reconcile a significant difference in τ_R in the two states. The possibility exists in which excited-state reactions such as those involving electron and proton transfer occur with an appreciable rate in the Ca^{2+}-saturated regulatory domain, whereas these reactions are negligible in the apo regulatory domain. These interactions between excited indole and functional groups in close proximity can participate in nonradiative decay processes (Petrich et al., 1987; Yu et al., 1992). In general, such excited-state reactions are expected to be accompanied by a negative amplitude in the intensity decay or a red-shift of the emission of the long component. There is no evidence of a negative amplitude in the decay of F22W, and the emission spectrum associated with the long decay component is not red-shifted (Fig. 9). A recently proposed "reversible kinetics" model can account for excited-state electron/proton transfer reactions giving rise to nonexponential decay without a negative amplitude (Van Gilst et al., 1994). Since the molecular graphics show no significant alteration of the amino acid side-chain packing around Trp-22 between the apo and Ca^{2+}-saturated N-domain, it seems unlikely that these potential excited-state reactions would be eliminated in the absence of bound Ca^{2+}. Taken together, the available information does not support the possibilities of solvent relaxation or excited-state reactions as the dominant origin of the biexponential decay observed in the presence of bound activator Ca^{2+}.

An alternative interpretation of the origin of the biexponential decay in the 4-Ca state is ground-state heterogeneity. The decay results suggest two Trp-22-resolved conformational states. We have constructed DAS for F22W as described in Materials and Methods, using the decay times of the tryptophan residue determined at a number of wavelengths across the emission band. The two resolved spectra are shown in Fig. 9 together with the steady-state spectra for the 2-Mg and the 4-Ca states. The spectrum associated to the long lifetime has a maximum essentially the same as that in the steady-state spectrum (331 nm). The spectrum associated to the short lifetime is red-shifted to ~350 nm, a characteristic expected of tryptophan in a more aqueous environment, and this spectrum makes only a small contribution to the total quantum yield. These results are consistent with a very small red-shift of the steady-state spectrum and a substantial decrease in quantum yield in the 4-Ca state when compared with the 2-Mg state. The dominant emitting species of the Ca^{2+}-saturated N-domain is very similar to

TABLE 3 Fluorescence anisotropy decays of single-tryptophan TnC mutants

Mutant	Ligand	ϕ_1 (ns)	r_1	ϕ_2 (ns)	r_2	r_o	θ (deg)
F22W	Mg^{2+}	8.31 ± 0.25	0.120 ± 0.003	0.80 ± 0.30	0.023 ± 0.005	0.143 ± 0.008	19.5 ± 4.1
	Ca^{2+}	11.59 ± 0.45	0.119 ± 0.003	1.16 ± 0.33	0.022 ± 0.003	0.141 ± 0.006	19.1 ± 2.7
M-1	Mg^{2+}	8.06 ± 0.49	0.118 ± 0.006	0.80 ± 0.51	0.026 ± 0.005	0.144 ± 0.011	20.7 ± 4.4
	Ca^{2+}	10.12 ± 0.47	0.102 ± 0.004	1.46 ± 0.45	0.023 ± 0.003	0.125 ± 0.007	20.9 ± 3.1
M-2	Mg^{2+}	6.64 ± 0.19	0.086 ± 0.002	0.38 ± 0.07	0.059 ± 0.010	0.145 ± 0.012	33.1 ± 4.2
	Ca^{2+}	7.33 ± 0.27	0.073 ± 0.001	0.33 ± 0.04	0.079 ± 0.010	0.152 ± 0.011	38.8 ± 3.3
M-3	Mg^{2+}	8.36 ± 0.40	0.079 ± 0.002	0.71 ± 0.09	0.058 ± 0.004	0.137 ± 0.006	33.9 ± 1.9
	Ca^{2+}	10.80 ± 0.31	0.099 ± 0.001	0.56 ± 0.09	0.048 ± 0.006	0.147 ± 0.007	28.9 ± 2.9

These measurements were carried out with ~5 μM protein at 23°C. Emission was isolated with a cutoff filter [Schott WG320 ($\lambda > 320$ nm)]. Other conditions are given in the legends to Tables 1 and 2. The errors for the two rotational correlation times (ϕ_1 and ϕ_2), the corresponding anisotropy values (r_1 and r_2), and the zero-time anisotropy (r_o) were the variance from the least-squares fitting. θ is the cone semiangle over which the tryptophan side chain moved and was calculated from $r_1/(r_1 + r_2) = (1/4)\cos^2\theta(1 + \cos\theta)^2$ (Lipari and Szabo, 1982). The uncertainty for θ was calculated from the theory of propagation of random error.

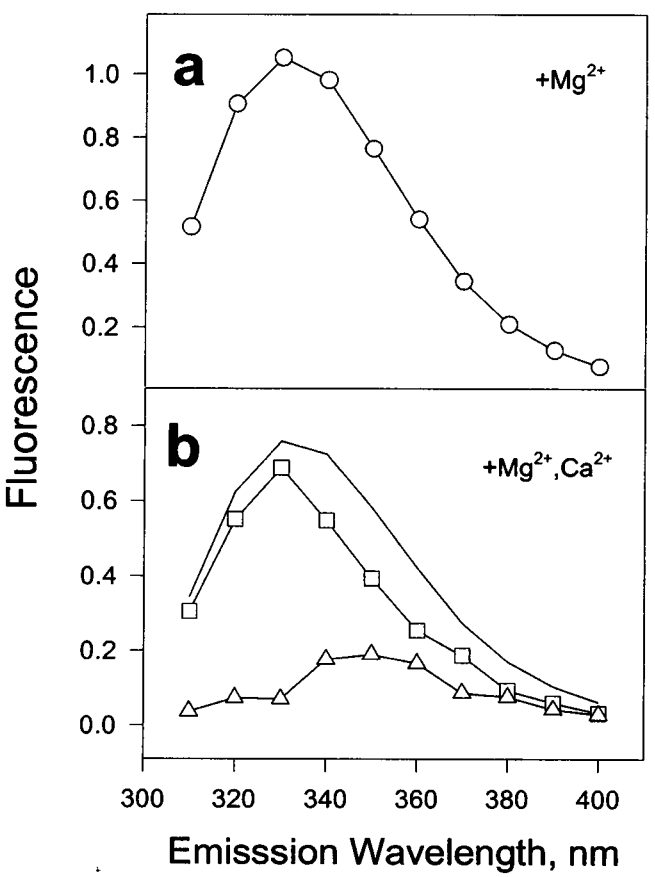

FIGURE 9 Decay-associated emission spectra of Trp-22 in F22W. (*a*) The steady-state spectrum obtained in the presence of Mg^{2+}, and (*b*) in the presence of Mg^{2+} + Ca^{2+}. The top curve is the steady-state spectrum; the two lower curves are the DAS associated to the long lifetime (*squares*) and the short lifetime (*triangles*).

the homogeneous, one-state apo N-domain in which Trp-22 is sufficiently protected from solvent interaction, and the other Ca^{2+}-bound emitting species appears to be substantially more exposed to the solvent. We note that Trp-22 is located in the middle of helix A and seven residues away from the N-terminal end of Ca^{2+}-binding loop 1. Its location is in close proximity to the two putative EF-hands of the Ca^{2+}-saturated N-domain. It is not clear whether one species would correspond to the N-domain with only one site occupied, and the other species to occupation of a second site. A Ca^{2+} titration of the DAS would be needed to further address this issue.

A mutant of TnC (F29W), in which the tryptophan is located at the C-terminal end of helix A and immediately adjacent to the first Ca^{2+}-binding loop, was previously reported (Pearlstone et al., 1992a). A preliminary report showed triexponential and biexponential intensity decays in the absence and presence of Ca^{2+}, respectively (Clark and Szabo, 1993). Multiple decay times have been observed in many single-tryptophan peptides and proteins, and these decays were rationalized in terms of the χ_1 and/or χ_2 rotamers resulting from rotation of the indole ring about the C_α—C_β and/or the C_β—C_γ bonds (Donzel et al., 1974; Szabo and Rayner, 1980). In recent studies, direct correlation between the resolved tryptophan lifetimes and tryptophan rotamers have been demonstrated (Philips et al., 1988; Tilstra et al., 1990; Ross et al., 1992; Dahms et al., 1993). Whether tryptophan side-chain rotamers are present in a given protein is dependent upon structural constraints imposed on the side chain and specific interactions of the indole ring with other side chains and the polypeptide backbone. The x-ray structure of TnC clearly indicates large differences in the environment of the tryptophan between F22W and F29W, and the different observed decay properties of the two proteins must be related to structural differences (She et al., 1997). It is tempting to suggest that the well-defined single lifetime of F22W indicates the absence of multiple rotamers and that the previously reported multiple lifetimes of F29W reflect the presence of rotamers. On this basis, the appearance of a second lifetime for the 4-Ca state of F22W could be rationalized in terms of two ground-state conformations of the N-domain in which the tryptophan side chain exists in two of the three possible χ_1 rotamer conformations.

The decay of Trp-52 is more complex than that of Trp-22. In the 2-Mg state, the intensity decay is clearly biexponential with a 4-ns component and a short component in the range of 1–2 ns. Trp-52, which is located in a loop linking

helices B and C, is fully exposed to solvent and not constrained in the x-ray structure. This environment may give rise to a ground-state heterogeneity of Trp-52, and the observed two lifetimes may be due to the presence of two rotamers. The lower quantum yield (0.14) and the shorter mean lifetime of M-2 in the absence of bound activator Ca^{2+} relative to F22W and M-1 result from a combination of a 60% reduction in the radiative decay rate and a twofold increase in the nonradiative rate (Table 1). These results are consistent with changes in K_{SV} and k_q when tryptophan is moved from position 22 to 52. In the presence of bound Ca^{2+} at the N-terminal domain, the quantum yield is slightly reduced with no detectable change in the spectral maximum. Both the Stern-Volmer dynamic quenching constant and the bimolecular quenching constant, however, are reduced by >25%. These results are consistent with a less solvent-accessible Trp-52 in the 4-Ca state than in the 2-Mg/2-Ca state. This conclusion is not borne out in the modeled 4-Ca structure of TnC, which predicts increased exposure of several residues in helix B and the linker between helices B and C induced by bound Ca^{2+} in the N-domain. Two recent studies have reported Ca^{2+}-induced environmental changes of residues 48 and 47 in TnC from skeletal (Pearlstone et al., 1992b) and cardiac (Howarth et al., 1995) muscle, respectively, that are also in a direction opposite to that predicted by the 4-Ca computer model.

The constructed DAS for Trp-52 in M-2 are shown in Fig. 10. The dominant emitting species of the 2-Mg state has a spectrum very similar to the steady-state spectrum and is identified with the long lifetime. The short decay component contributes <12–13% to the overall steady-state spectrum. The present DAS data do not accurately define the wavelength of maximum emission of the short lifetime component. For the 4-Ca state (Fig. 10 *b*), two well-defined DAS spectra with significant contributions have been obtained. The new decay time (2 ns) is responsible for the unshifted spectrum, whereas the spectrum associated to the 6-ns component is red-shifted by ~10 nm to 360 nm. The third and shortest lifetime has a very minor contribution (~6%) to the total quantum yield. The origin of the three lifetimes could be rationalized by ground-state heterogeneity with three tryptophan rotamers. The presence of these conformers reflects Ca^{2+}-induced conformations of the regulatory N-domain.

The emission properties of Trp-90 in M-3 show features that are different from tryptophan in the other two positions. Trp-90 is located at the N-terminal end of the central helix and approximately equidistant from the two Ca^{2+}-specific sites in the N-terminal domain and the two Ca/Mg sites in the C-terminal domain. In the 2-Mg state, the two Ca/Mg sites in the C-terminal domain are saturated. The emission spectrum of M-3 is significantly blue-shifted compared to NATA. The low quantum yield (0.12) is due to a 30% smaller radiative decay rate and a 2.5-fold increase in the nonradiative rate when compared with F22W. The relatively small value of k_q (1.76×10^9 M^{-1} s^{-1}) and the spectral maximum (345 nm) suggest that Trp-90 in M-3 is

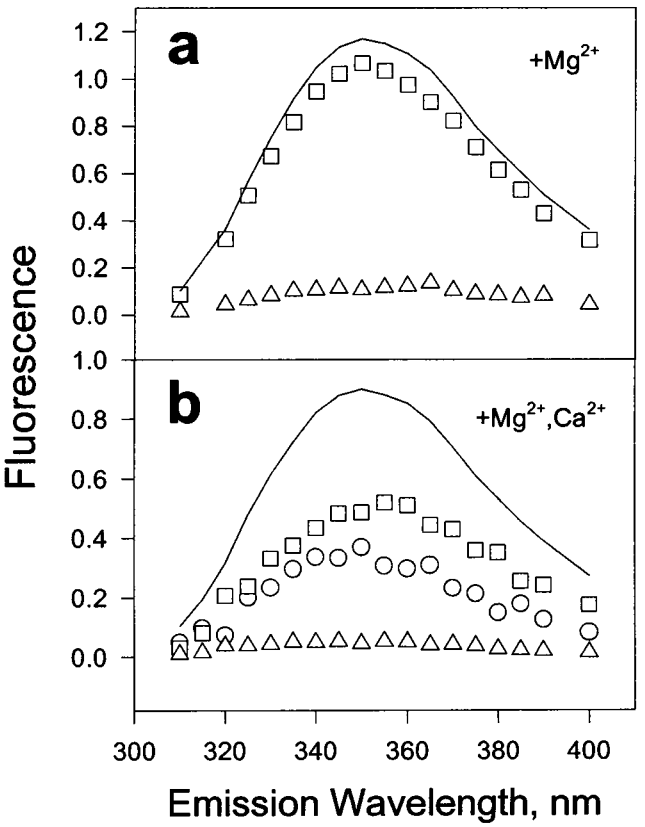

FIGURE 10 Decay-associated emission spectra of Trp-52 in mutant M-2. (*a*) In the presence of Mg^{2+}. Top curve, the steady-state spectrum; squares, the DAS associated to the long lifetime; triangles, the DAS associated to the short lifetime. (*b*) In the presence of Mg^{2+} and Ca^{2+}. The top curve is the steady-state spectrum; the DAS associated to the three lifetimes: the long lifetime (*circles*), the intermediate lifetime (*squares*), and the shortest lifetime (*triangles*).

partially shielded from solvent, comparable to Trp-90 in F22W. This is not compatible with the molecular graphics, which show Trp-90 to be widely accessible to solvent. If TnC is flexing in the region of the central helix and less extended in solution than predicted by crystallography, Trp-90 could be protected from solvent via transient contacts with other side chains. These interactions may give rise to an increase in the nonradiative rate, thus resulting in a low quantum yield (0.12), The binding of Ca^{2+} at the regulatory sites modifies these interactions such that the nonradiative rate is reduced from 28.9×10^7 to 19.8×10^7 s^{-1} with a 2-nm blue shift and a 40% increase in quantum yield. The absorption spectrum of M-3 shows a reproducible red-shift in the 280–290 nm region upon the addition of Ca^{2+} to saturate the regulatory sites (data not shown). Since this absorption band is an $n \rightarrow \pi^*$ transition, the spectral shift is in agreement with the observed Ca^{2+}-induced blue-shift of the emission spectrum, indicating a less polar environment of Trp-90 in the 4-Ca state. Several other lines of evidence suggest a less extended solution conformation of skeletal muscle TnC (Heidorn and Trewhella, 1988; Wang et al., 1989) and possible interaction between the N- and

C-domains (Wang et al., 1993; Mehler et al., 1991). The present results provide additional support of a less extended model of TnC and suggest considerable shielding of the N-terminal segment of the central helix from solvent interaction. It is of interest to note that the emission properties of Trp-90 in M-3 are very similar to those of calmodulin mutant S81W SYNCAM. The tryptophans of the two proteins are in equivalent positions on the central helix. The Ca^{2+}-induced spectral changes observed with calmodulin S81W are in apparent contradiction to the solvent exposure of Trp-81 shown on the molecular graphics (Chabbert et al., 1991). This deviation is similar to that observed with Trp-90 in the present work.

The DAS constructed for M-3 from triexponential fits of decay data obtained in the presence of Mg^{2+} are shown in Fig. 11 *a*. The spectrum associated to the longest lifetime (5 ns) is unshifted from the steady-state spectrum, whereas the spectrum associated to the intermediate lifetime (2 ns) appears to be slightly red-shifted, although the data are not sufficient to define the maximum of the spectrum. The spectrum associated to the shortest lifetime (≤1 ns) is not well defined and contributes less than ~10% to the entire spectrum. Figure 11 *b* shows the two resolved DAS obtained in the presence of Mg^{2+} plus Ca^{2+}. The major contribution is from the long decay component, and this spectrum is unshifted. The minor component is associated to the short lifetime with a small red-shift. The two Trp-90 conformers in the 4-Ca state may be in a very similar environment. Since Trp-90 detects Ca^{2+} binding to both sets of sites in the N-domain and C-domain (data not shown), the three resolved DAS may reflect the local conformations of Trp-90 modulated by bound Mg^{2+} at the C-domain Ca/Mg sites. Similarly, the two resolved DAS obtained in the presence of both Mg^{2+} and Ca^{2+} may reflect contributions of both sets of binding sites to the Trp-90 conformation.

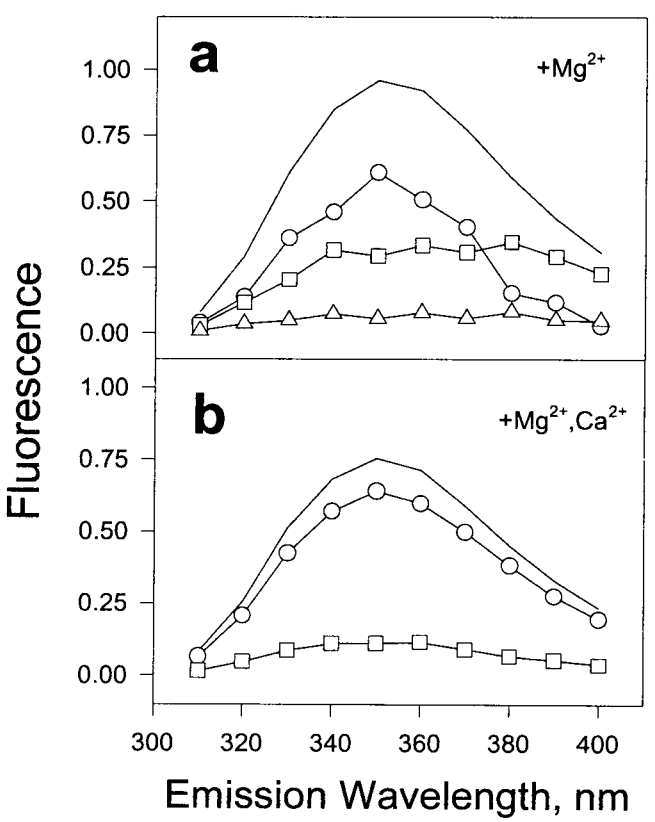

FIGURE 11 Decay-associated emission spectra of Trp-90 in mutant M-3. (*a*) In the presence of Mg^{2+}. The top curve is the steady-state spectrum. Circles, DAS associated to the longest lifetime; squares, DAS associated to the intermediate lifetime; triangles, DAS associated to the shortest lifetime. (*b*) In the presence of Mg^{2+} + Ca^{2+}. The top curve is the steady-state spectrum. Circles, DAS associated to the long lifetime; squares, DAS associated to the short lifetime.

The anisotropy decays of Trp-22 in F22W and M-1 are essentially indistinguishable from each other, and regardless of the absence or presence of cation the decay is adequately described by two rotational correlation times. If the assumption is made that TnC can be approximated by a rigid prolate ellipsoid of revolution and has a hydration value of 0.4–0.5 g of water/g protein (Hubbard et al., 1988) and an axial ratio of 2–3 on the basis of the x-ray structure, two theoretical rotational correlation times can be readily calculated (Cheung et al., 1991). The calculated short correlation time (ϕ_b) corresponding to the rotation of the short axis is considerably longer than the observed short correlation time (ϕ_2 = 0.8–1.5 ns). This result rules out the possibility that ϕ_2 corresponds to ϕ_b and suggests that ϕ_2 reflects the mobility of the tryptophan side chain. This mobility occurs on the subnanosecond regime and may result from motions about the C_β—C_γ bond. It is possible that motions about other bonds may also contribute to the observed mobility, but fluorescence data alone cannot provide an answer. The calculated long correlation time (ϕ_a) corresponding to the rotation of the long axis is expected in the range of 8–19 ns. The observed long correlation time (ϕ_1) in the presence of Mg^{2+} (8.31 ns) is comparable to the harmonic mean (ϕ_h) of the two calculated correlation times and can be attributed to the global motion of the entire protein. The presence of bound Ca^{2+} at the N-terminal domain does not appear to have a large effect on the motion of the indole ring, but lengthens the global correlation time ϕ_1 by ~3 ns, suggesting a less compact or a more elongated hydrodynamic shape.

The anisotropy decay of Trp-52 in M-2 yields correlation times that are considerably smaller than those derived from Trp-22. ϕ_2 is reduced to values <0.4 ns, whereas ϕ_1 decreases to the range of 6.6–7.3 ns. The reduction in ϕ_2 is accompanied by a larger cone semiangle (θ = 33°) as compared with that of Trp-22 (19°). In addition, Ca^{2+} increases this angle by 5–6°. With Trp-90 in M-3, ϕ_2 is also reduced compared with Trp-22, but the global correlation time is not altered. The change in ϕ_2 is accompanied by an increase in the cone semiangle to 34°. The effect of bound activator Ca^{2+} is a decrease of 5° in the cone semiangle, a change in the opposite direction of that observed with Trp-52. The differences in the values of ϕ_2 and the semi-

angle of the tryptophan side chain in the three positions provide additional structural information about the three sites in TnC. The longer ϕ_2 values and smaller cone semiangles of Trp-22 are consistent with the other findings that Trp-22 is in a more restricted environment. Although Trp-22 is in a close proximity to the two Ca^{2+} sites in the N-domain, saturation of these sites has only a small effect on its observed mobility. The observed Ca^{2+}-induced increase in the global correlation time must result from reorientation of one or more of the helices in the N-domain to produce a more asymmetric hydrodynamic shape. The value of ϕ_2 for M-2 is a factor of two smaller than that of F22W, in agreement with the molecular graphics that Trp-52 is relatively unrestricted in its environment. The smaller global correlation time sensed by Trp-52 is consistent with this internal flexibility. Although Ca^{2+} induces a small increase (<1 ns) in ϕ_1, its value is considerably smaller than that observed with Trp-22. A possible reason for this is that the indole motion of Trp-52 occurs over a larger angular range, which may be responsible for the observed depolarization. Although the cone semiangle of Trp-90 is comparable to that of Trp-52, the short correlation time ϕ_2 is a factor of two larger than that of Trp-52. The decrease in the cone semiangle by bound Ca^{2+} coupled with the larger short correlation time may minimize the depolarization that is seen with Trp-52. Consequently, the global correlation time sensed by Trp-90 is very comparable to that sensed by Trp-22. The present analysis indicates that the global correlation time obtained from time-resolved fluorescence anisotropy must be interpreted with caution. If the fluorophore is located in a flexible region of the protein or has considerable mobility, the observed value of the global correlation time may be shortened by local motions. On the other hand, fluorophores located in relatively immobile regions report correlation times that reflect more accurately the global motion of the protein.

By using single tryptophans located in different regions of the protein, we have investigated local and global conformations of TnC and examined the effects of activator Ca^{2+} on these conformations. The observed Ca^{2+}-induced conformations provide insights into the role of TnC in calcium activation. Some of these conformations may be related to the known Ca^{2+}-dependent enhanced interaction between TnC and TnI and play a role in the calcium switch of muscle activation. The present results show environmental changes of tryptophans located in two different positions that are not in agreement with the molecular graphics based on the modeled structure of the Ca^{2+}-saturated regulatory domain. These results also suggest an increase in the asymmetry of TnC resulting from binding of activator Ca^{2+}. Whether these conformational features can be related to the activation mechanism is not known. Additional studies with reconstituted troponin or the TnC-TnI complex will be required to address this issue.

The authors thank Prof. Thomas Nordlund for assistance in several aspects of the operation of the dye laser system used in this work.

This work was supported by National Institutes of Health Grants AR25193 and HL52508 (to H.C.C.) and PKU HL44094 (to P.K.U.), and a Postdoctoral Fellowship from the Muscular Dystrophy Association (to W.J.D.).

REFERENCES

Bakhshiev, N., G. Yu, T. Mazuerenko, and I. V. Piterskaya. 1966. Luminescence decay in different portions of the luminescence spectrum of molecules in viscous solution. *Opt. Spectrosc.* 21:307–309.

Chabbert, M., T. J. Lukas, D. M. Watterson, P. H. Auxelsen, and F. G. Prendergast. 1991. Fluorescence analysis of calmodulin mutants containing tryptophan: conformational changes induced by calmodulin-binding peptides from myosin light chain kinase and protein kinase II. *Biochemistry.* 30:7615–7639.

Cheung, H. C., C.-K. Wang, and N. A. Malik. 1987. Interaction of troponin subunits: free energy of binary and ternary complexes. *Biochemistry.* 26:5904–5907.

Clark, I. D., and A. G. Szabo. 1993. A time-resolved fluorescence study of TnC single tryptophan mutant, F29W. *Biophys. J.* 64:135*a*. (Abstr.).

Dahms, T. E. S., K. J. Willis, and A. G. Szabo. 1993. Fluorescence decay kinetics of a tryptophanyl residue in a protein crystal. *Biophys. J.* 64:55*a*. (Abstr.).

Davis, D. M., D. McLoskey, D. J. Birch, R. M. Swart, P. R. Gellert, and R. S. Kittlety. 1994. Fluorescence studies of tryptophan and human serum albumin (HSA) in AOT reverse micelles. *SPIE PROC* 2137: 331–324.

DeToma, R. P., J. H. Easter, and L. Brand. 1976. Dynamic interactions of fluorescence probes with the solvent environment. *J. Am. Chem. Soc.* 98:5001–5007.

Donzel, B., P. Gauduchon, and Ph. Wahl. 1974. Study of the conformation in the excited state of two tryptophanyl diketopiperazines. *J. Am. Chem. Soc.* 96:801–808.

Eftink, M. R. 1991. Fluorescence quenching: theory and applications, *In* Topics in Fluorescence Spectroscopy, Vol. 2. J. R. Lakowicz, editor. Plenum Press, New York. 53–126.

Eftink, M. R., and C. A. Ghiron. 1976. Exposure of tryptophanyl residues in proteins. Quantitative determination by fluorescence quenching studies. *Biochemistry.* 15:672–680.

Fabiato, A. 1988. Computer programs for calculating total from specified free and free from total ionic concentrations in aqueous solutions containing multiple metals and ligands. *Methods Enzymol.* 157:378–417.

Grinvald, A., and I. Z. Steinberg. 1974. On the analysis of fluorescence decay kinetics by the method of least-squares. *Anal. Biochem.* 59: 583–589.

Heidorn, D. B., and J. Trewhella. 1988. Comparison of the crystal and solution structures of calmodulin and troponin C. *Biochemistry.* 27: 909–915.

Herzberg, O., and M. N. G. James. 1985. Structure of the calcium regulatory protein troponin-C at 2.8 Å resolution. *Nature.* 313:653–659.

Herzberg, O., J. Moult, and M. N. G. James. 1986. A model for the Ca^{2+}-induced conformational transition of troponin C. *J. Biol. Chem.* 261:2638–2644.

Howarth, J. W., G. A. Krudy, X. Lin, J. A. Putkey, and R. Rosevear. 1995. An NMR spin-labeled study of the effects of binding calcium and troponin I inhibitory peptide to cardiac troponin C. *Protein Sci.* 4:671–680.

Hubbard, S. R., K. D. Hodgson, and S. Doniach. 1988. Small-angle x-ray scattering investigation of the solution structure of troponin C. *J. Biol. Chem.* 263:4151–4158.

Kretsinger, R. H., and C. E. Nockolds. 1973. Carp muscle calcium-binding protein. Structure determination and general description. *J. Mol. Biol.* 248:3313–3326.

Lakowicz, J. R., and H. Cherek. 1980. Dipolar relaxation in proteins in the nanosecond time scale observed by wavelength-resolved phase fluorometry of tryptophan fluorescence. *J. Biol. Chem.* 255:831–834.

Leavis, P. C., S. S. Rosenfeld, J. Gergely, Z. Grabarek, and W. Drabikowski. 1978. Proteolytic fragments of troponin C. Localization of high and low affinity Ca^{2+} binding sites and interactions with troponin I and troponin T. *J. Biol. Chem.* 253:5452–5459.

Liao, R., C.-K. Wang, and H. C. Cheung. 1992. Time-resolved tryptophan emission study of cardiac troponin I. *Biophys. J.* 63:986–995.

Lipari, G., and A. Szabo. 1982. Model-free approach to the interpretation of nuclear magnetic resonance relaxation in macromolecules. 1. Theory and range of validity. *J. Am. Chem. Soc.* 104:4546–4558.

Mehler, E. L., J. L. Pascual-Ahuir, and H. Weinstein. 1991. Structural dynamics of calmodulin and troponin C. *Protein Sci.* 4:625–637.

Parker, C. A., and W. T. Rees. 1960. Correction of fluorescence spectra and measurement of fluorescence quantum efficiency. *Analyst (London).* 85:587–600.

Pearlstone, J. R., T. B. Borgfrod, M. Chandra, K. Oikawa, C. M. Kay, O. Herzberg, J. Moult, A. Herklotz, F. Reinach, and L. S. Smillie. 1992a. Construction and characterization of a spectral probe mutant of troponin C: application to analyses of mutants with increased Ca^{2+} affinity. *Biochemistry.* 31:6545–6553.

Pearlstone, J. R., W. D. McCubbin, C. M. Kay, B. D. Sykes, and L. B. Smillie. 1992b. Spectroscopic analysis of a methionine-48 to tyrosine mutant of chicken troponin C. *Biochemistry.* 31:9703–9708.

Petrich, J. W., J. W. Longworth, and G. F. Fleming. 1987. Internal motion and electron transfer in proteins: a picosecond fluorescence study of three homologous azurins. *Biochemistry.* 26:2711–2722.

Philips, L. A., S. P. Webb, S. J. Martinez III, G. R. Fleming, and D. H. Levy. 1988. Time-resolved spectroscopy of tryptophan conformers in a supersonic jet. *J. Am. Chem. Soc.* 110:1352–1355.

Potter, J. D., and J. Gergely. 1975. The calcium and magnesium binding sites on troponin and their role in the regulation of myofibrillar ATPase. *J. Biol. Chem.* 250:4628–4633.

Ross, J. B. A., H. B. Wyssbrod, R. A. Porter, G. P. Schwartz, C. A. Michaels, and W. R. Laws. 1992. Correlation of tryptophan fluorescence intensity decay parameters with ^{1}H-NMR-determined rotamer conformations: [tryptophan^2]oxytocin. *Biochemistry.* 31:1585–1594.

She, M., W.-J. Dong, P. K. Umeda, and H. C. Cheung. 1997. Single-tryptophan mutants of troponin C from chicken skeletal muscle. An optical probe of the conformation of the regulatory domain. *Euro. J. Biochem.* In press.

She, M., P. K. Umeda, and H. C. Cheung. 1995. Intramolecular distances in troponin C mutants. *Biophys. J.* 68:58*a*. (Abstr.).

Strynadka, N. C. J., and M. N. G. James. 1989. Crystal structures of the helix-loop-helix calcium-binding proteins. *Annu. Rev. Biochem.* 58: 951–988.

Sundaralingam, M., R. Bergstrom, G. Strasburg, R. T. Rao, P. Roychowdhury, M. Greaser, and B. C. Wang. 1985. Molecular structure of troponin C from chicken skeletal muscle at 3-Å resolution. *Science.* 227:945–948.

Szabo, A. G., and D. M. Rayner. 1980. Fluorescence decay of tryptophan conformers in aqueous solution. *J. Am. Chem. Soc.* 102:554–563.

Tao, T., B-J. Gong, and P. C. Leavis. 1990. Calcium induced movement of troponin I relative to actin in skeletal muscle thin filaments. *Science.* 247:1339–1341.

Tilstra, L., M. C. Sattler, W. R. Cherry, and M. D. Barkley. 1990. Fluorescence of a rotationally constrained tryptophan derivative, 3-carboxy-1,2,3,4-tetrahydro-2-carboline. *J. Am. Chem. Soc.* 112:9176–9182.

Valeur, B., and G. Weber. 1977. Resolution of the fluorescence excitation spectrum of indole into its ^1L_a-^1L_b excitation bands. *Photochem. Photobiol.* 25:441–444.

Van Gilst, M., C. Tang, A. Roth, and B. Hudson. 1994. Quenching interactions and nonexponential decay: tryptophan 138 of bacteriophage T4 lysozyme. *J. Fluorescence.* 4:203–208.

Wahl, Ph., and J. C. Auchet. 1972. Résolution des spectres de fluorescence au moyen des déclines. Application à l'étude de la sérum albumine. *Biochim. Biophys. Acta.* 285:99–117.

Wang, C.-K., J. Lebowitz, and H. C. Cheung. 1989. Acid-induced dimerization of skeletal troponin C. *Protein.* 6:424–430.

Wang, C.-K., R. Liao, and H. C. Cheung. 1993. Rotational dynamics of skeletal muscle troponin C. *J. Biol. Chem.* 268:16471–16477.

Ware, W. R., S. K. Lee, G. J. Brant, and P. P. Chow. 1971. Nanosecond time-resolved emission spectroscopy: spectral shifts due to solvent-excited solute relaxation. *J. Chem. Phys.* 54:4729–4737.

Werner, T. C., and L. S. Foster. 1979. The fluorescence of tryptophanyl peptides. *Photochem. Photobiol.* 29:905–914.

Yu, H.-T., W. J. Colucci, M. I. McLaughlin, and M. D. Barkley. 1992. Fluorescence quenching in indoles by excited-state proton transfer. *J. Am. Chem. Soc.* 114:8449–8454.